Application of SbpRAY for simulation and optimization of a heliostat field and cavity receiver

Cite as: AIP Conference Proceedings **2303**, 160006 (2020); https://doi.org/10.1063/5.0030257
Published Online: 11 December 2020

Vanessa Schönfelder, and Thomas Keck

Application of SbpRAY for Simulation and Optimization of a Heliostat Field and Cavity Receiver

Vanessa Schönfelder [1, a)] and Thomas Keck [1, b)]

[1] *schlaich bergermann partner, sbp sonne gmbh, Schwabstr. 43, 70197 Stuttgart, Germany*

[a)] Corresponding author: v.schoenfelder@sbp.de
[b)] t.keck@sbp.de

Abstract. This paper discusses the usage of sbpRAY for the optimization of a cavity receiver. New features have been implemented into the program for this purpose. A case study is presented which combines sbpRAY with Rhino and Grasshopper. The example is taken from Next-CSP[1], a research project investigating a high temperature solar thermal power plant with a cavity receiver which uses solid particles as heat transfer medium and as a storage material [1]. The influence of several parameters on the output variables is investigated.

INTRODUCTION

In the field of high temperature receivers of Central Receiver Systems, losses are dominated by IR radiation since it is dependent on temperature to the power of four (T^4). To prevent excessive radiation losses a cavity is necessary, which adds many geometry variables and makes optimization demanding. All loss parameters need to be considered, the solar field has to be modelled and an efficient aim point strategy (APS) needs to be applied which is particularly challenging. This highly complex multi-parameter optimization requires a powerful and very flexible tool.

Gebreiter et al. introduced sbpRAY, a tool developed by sbp sonne gmbh (sbp), for simulation of heliostat fields and receivers for large scale CSP plants [2]. The present work focuses on the application of sbpRAY for high temperature systems with cavity receivers. The optimization of the cavity receiver is realized via coupling sbpRAY with Grasshopper and Rhino. Rhino is a powerful 3D free form surface modeler [3]. It is based on NURBS curves, mathematical curves that allow the user to display any 3D geometry [3]. Grasshopper is a visual programming tool that enables intuitive parametric modelling [3]. It is embedded into Rhino [3].

For the purpose of optimizing cavity receivers sbpRAY has been further developed. The new features of the software and a case study are presented. The case study is taken from a European research project called Next-CSP[1]. In the scope of this project, a high temperature solar thermal power plant with a cavity receiver was simulated. The overall aim of the project is the analysis of solid particles as storage material and heat transfer medium [1]. This allows one heat transfer step to be eliminated within which heat would be lost. It is hoped that a significant increase in the efficiency of the power plant can be achieved thereby [1]. To verify the technology, a pilot solar loop of 4 MW_{th} is built into the Themis solar tower in France [1]. Simulations for a large system consisting of several towers and solar fields with an overall thermal energy output of 150 MW_{th} are also part of the project. The simulations consider individual system parts as well as the overall plant [1]. A thermal output of roughly 44 MW_{th} into the absorber tubes was set as the goal for the cavity receiver. The high performance Stellio heliostat was considered for simulation of the heliostat field [4].

[1] Next-CSP is a project that has received funding from the European Union's Horizon 2020 research and innovation programme under grant agreement No 727762

SolarPACES 2019
AIP Conf. Proc. 2303, 160006-1–160006-11; https://doi.org/10.1063/5.0030257
Published by AIP Publishing. 978-0-7354-4037-1/$30.00

EXTENDING SBPRAY FOR SIMULATION OF A CAVITY RECEIVER

sbpRAY is a raytracing software that enables simulation and design of a concentrating solar thermal power (CSP) plant. Relevant site conditions such as topography and atmospheric conditions can be inserted just like mirror and receiver configurations. All common loss factors are considered. The efficiencies of a solar field can be read out for the whole field as well as for each individual heliostat. Shading, blocking, etc. are all analysed. Regarding the receiver, each surface can be evaluated separately. Receiver power and flux are provided in detail. [2]

A new feature was implemented in sbpRAY making it possible to simulate multiple reflections from the cavity walls inside of a cavity receiver. The reflection behaviour can be set for each receiver surface individually. Diffuse as well as specular reflection with variable scattering and the maximum number of reflections can be chosen, using angular distributions provided by J. Greenwood [5].

A further newly implemented feature allows creating light sources of individual forms and positions. This permits the determination of view factors for geometries of all kinds. These are necessary for the calculation of IR radiation losses.

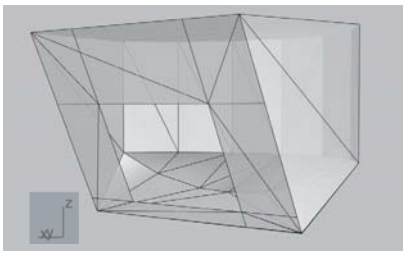

FIGURE 1. Next-CSP cavity receiver model in Rhino

Figure 1 shows the model of a cavity receiver for the Next-CSP project generated in Rhino. The absorber tubes are placed in front of the backwall.

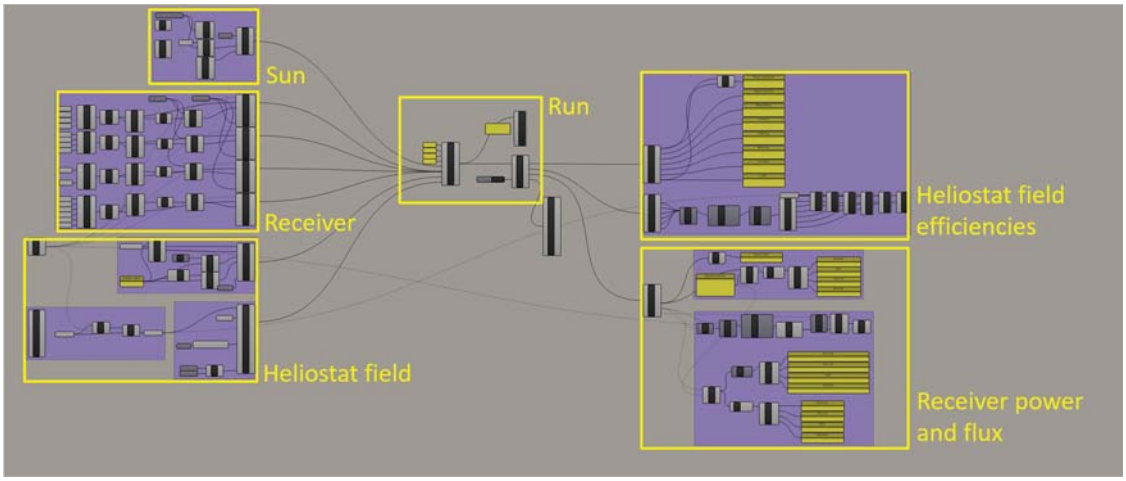

FIGURE 2. sbpRAY interface in Grasshopper

The basic structure of the sbpRAY interface in Grasshopper is illustrated in Fig. 2. There are several elements that present sbpRAY program parts. These can be combined with conventional Grasshopper elements. For example, the receiver itself can be designed in Rhino and inserted into Grasshopper using the Grasshopper interface, adjusted as desired with Grasshopper tools and fed into the sbpRAY element for receivers. Further information regarding the receiver such as reflectivity (diffuse or direct) can be fed into the receiver element. It is likewise possible to display output data visually and to analyse them further if required. As depicted in Fig. 2 the input information on sun, receiver and heliostats including aiming information are put together in the left part and are fed into the executing “run”

elements which are placed in the middle. The results on heliostat field efficiencies and receiver power and flux are collected on the right of the program interface.

By clicking on individual elements, contained geometric components are displayed in the Rhino surface. Figure 3 shows an exemplary display of heliostat sample output data. The Grasshopper element is activated in the Grasshopper window (a section of this window is visible on the right side of the image) and as a result the oriented heliostats become visible in the Rhino window (on the left side of the image).

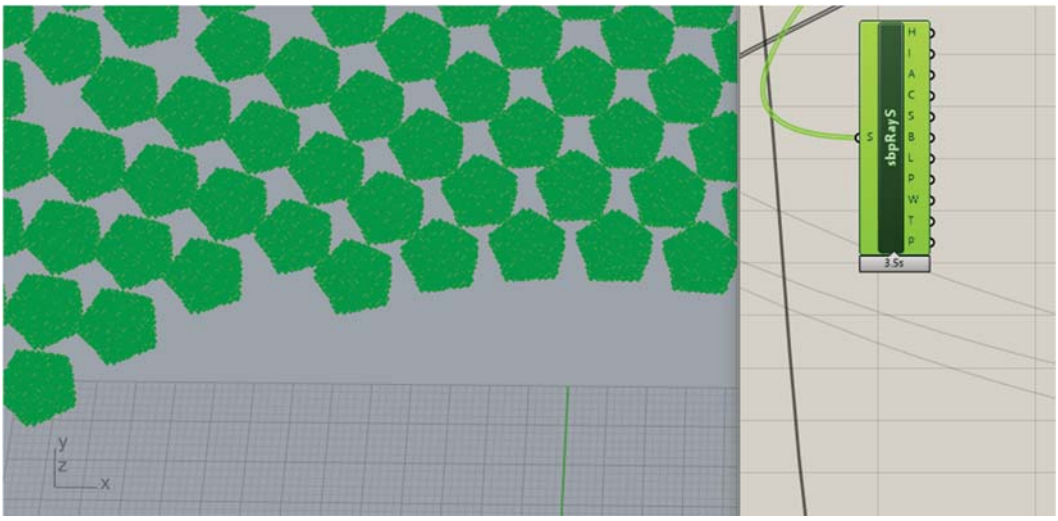

FIGURE 3. Visualisation of components contained in a Grasshopper element in Rhino

OPTIMIZATION OF A CAVITY RECEIVER WITH SBPRAY

As a first step, a rough model of the receiver was built in Rhino. This was done considering boundary conditions of the project such as absorber tube height and desired net output power. With sbpRAY and a simplified aiming strategy, a suitable solar field was established. The simulation of the solar field considers the sun positions over a whole year. First, an oversized, radially staggered field was generated. The most useful heliostats were then selected by evaluating the annual energy production for each heliostat. Next, a more detailed aiming strategy was implemented to meet the requirements of the absorber, regarding a special vertical flux profile as well as a horizontally homogenous distribution. The requirement of flux increasing from the top to the bottom of the panel was especially challenging to achieve. The flux limitations also had to be taken into account. The flexibility and efficient coupling between sbpRAY, Grasshopper and Rhino, enabled the APS to be varied fast and in an intuitive manner. The effect of any change is visible immediately and, as a consequence, logical conclusions can be drawn directly from observation. A broad range of functions are already available in Grasshopper that can be used to improve the implemented APS as well as receiver design. This is helpful for coarse adjustments and for fine tuning. For implementation of the APS only the design point was regarded. Figure 4 shows the receiver model with the aim points on the absorber as well as the resulting flux map.

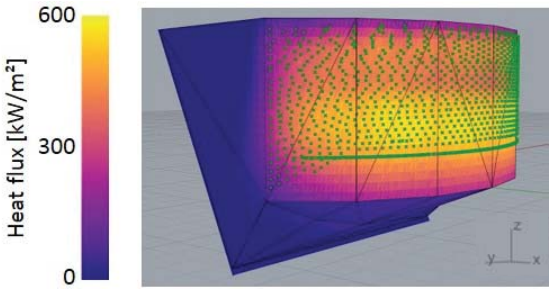

FIGURE 4. View from behind on absorber with aim points and flux map

The losses were calculated with simplified approaches. A presumed value was considered for the surface temperature of the absorber whereas the surface temperature on the inside and outside of the cavity walls were taken from the energy balance; which included convection, conduction and IR radiation losses of the complete receiver. One homogenous surface temperature for the inside of all cavity walls was assumed. Figure 5 and 6 illustrate the corresponding energy flow model.

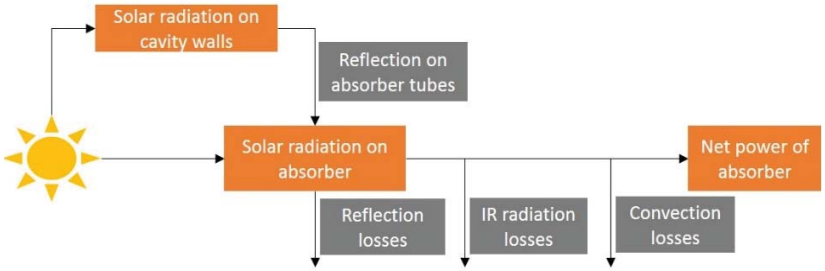

FIGURE 5. Energy flow model

Figure 6 shows the top view of the receiver. The yellow line represents the receiver walls with a hole that stands for the aperture. The red dots indicate the absorber tubes without showing the correct number nor scale. The numbers represent the following descriptions:

1. Solar radiation on absorber surface
2. Diffuse reflection from walls to absorber surface; multiple reflection considered
3. Solar radiation penetrating absorber tube spacing
4. Diffuse reflection from backwall to tubes
5. Absorber reflection; reflection loss partly regained by multiple diffuse reflections
6. Conduction losses
7. Convection and radiation losses through aperture

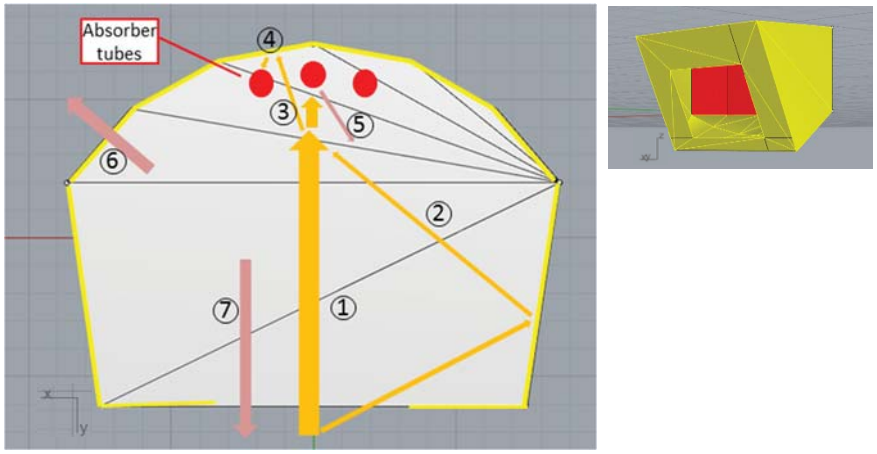

FIGURE 6. Graphical energy flow model

The loss model made certain simplifications due to the limited project budget. Apart from the simplifications already mentioned, losses due to spacing between the absorber tubes were estimated. They were calculated by taking the percentage of spacing (15 %) multiplied by the absorptivity of the backwall and assumed that another 15 % of the radiation that is reflected by the backwall passes through the spacing again and was not regained by further reflections. For the calculation of recovery of reflected radiation from the absorber, the absorber's cylindrical shape was simplified as a polygon, as was assumed for the radiation input.

A sensitivity analysis was performed on the impact of several factors on the losses. First, the effect of the absorber temperature was regarded, since this parameter is a presumed value. The result is shown in Fig. 7. As expected the

absorber temperature has a considerable impact on the losses. Especially radiative losses reduce with decreasing absorber temperatures, in the range of interest with an average of 27 % / 100 K. The vertical red line indicates the originally assumed absorber temperature of 950 °C. In general, the absorber temperature can be lowered by increasing the particle flow inside of the absorber tubes. The feasibility of increasing the particle flow still needs to be analysed considering stability of the flow as well as parasitic losses.

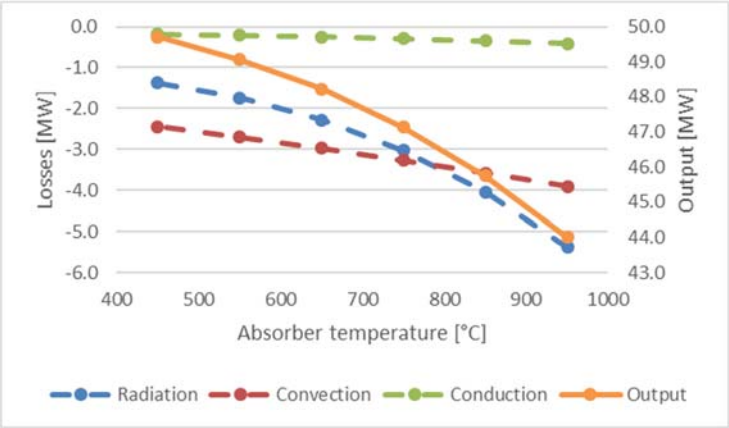

FIGURE 7. Impact of absorber temperature on losses

The impact of heat transfer surfaces on convective losses was also investigated. This parameter is affected by the cavity form and is related to the flow behaviour of the air inside of the cavity due to convective heating. Clausing [6] was taken as a basis for the convective flow patterns. As can be seen in Fig. 8, a stagnant zone is formed in the upper part of the cavity due to the temperature-dependent density of air which causes the air heated at the absorber to rise and stay behind the front wall of the cavity. This stagnant zone can be ignored for the calculation of convective losses. The remaining convection in the cavity was calculated using Clausing's formulas for the Nusselt factor.

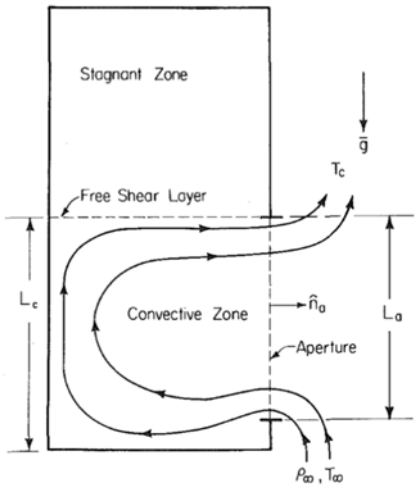

FIGURE 8. Convective flow patterns in cavity receivers according to Clausing [6]

The impact of convective surface size is shown in Fig. 9. The influence of the convection relevant part of backwall and absorber tubes is represented by the length L_a which defines the height of absorber tubes and backwall below the stagnant zone. Both convective areas are linearly dependent on this length.

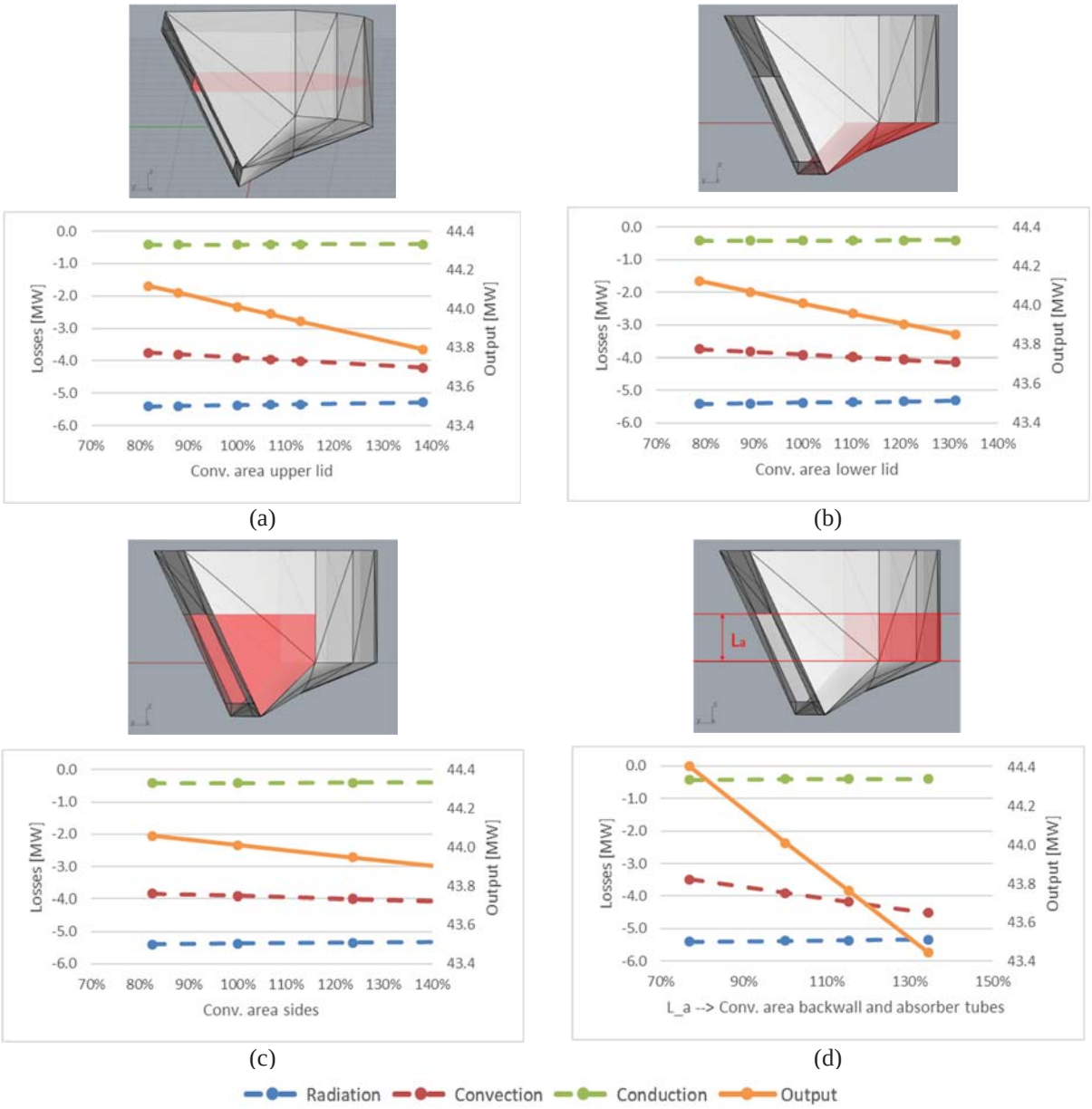

FIGURE 9. Impact of convective surface sizes on convective losses (a) upper lid (b) lower lid (c) side walls (d) height of backwall and absorber tubes L_a

When changing the partial convective surface areas, the following factors apply for the combined convection, radiation and conduction losses:

Upper lid: 0.6 % loss / 10 % area
Lower aperture frame: 0.03 % loss / 10 % area
Side walls: 0.3 % loss / 10 % area
Lower lid: 0.5 % loss / 10 % area
Backwall / absorber tube height L_a: 1.6 % loss / 10 % height

This indicates a rather small impact.

In addition, other studies on convection losses in cavity receivers were also regarded for verification purposes. Only a rough comparison was possible, as the cavity designs in those studies were considerably different. Nevertheless, the comparison showed results of the same order of magnitude by matching convective surfaces and surface temperatures. One study consulted for verification by Samanes et al. states the Clausing calculation as the most detailed one [7].

After adding losses to the simulation, the receiver geometry was optimized with the aim of maximizing the net output power. Due to the large number of parameters the geometry was first optimized manually to get a reasonable starting point. Several geometrical parameters were then optimized automatically. Potential for a more comprehensive optimization remains.

Important parameters are the distance between aperture and absorber tubes and the aperture tilt angle (the absorber tubes of the Next-CSP receiver can't be tilted but must be vertical). The distance is chosen in such a way that the aperture position and angle coincide with the crossing zone of the beam aim lines. Crossing zone in this case means the area in which the cross-section of an imaginary enclosure of the lines from each heliostat to the corresponding aim point on the absorber reaches its minimum. Figure 10 displays these aim lines. The afore mentioned parameters aperture tilt angle and distance between aperture and absorber tubes are displayed in red. The crossing zone can be identified by the constricted bundling of the lines approximately at the height of the aperture. Real beam size is not shown in this illustration.

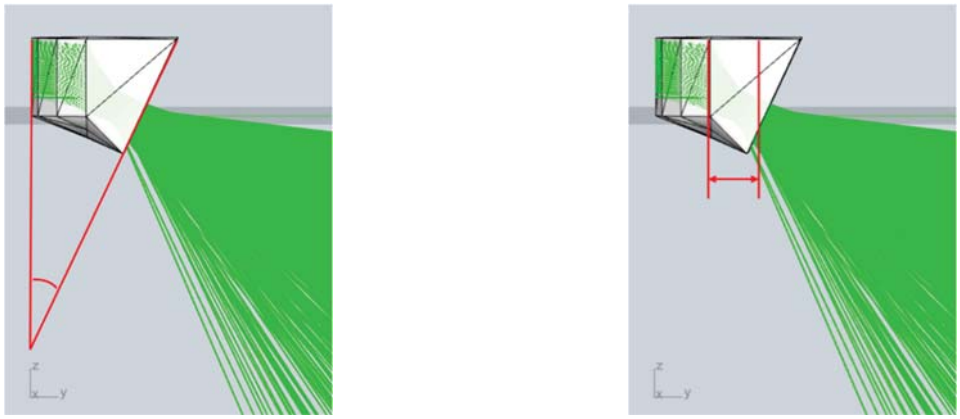

(a) (b)

FIGURE 10. Important geometrical parameters for cavity design (a) tilt angle (b) distance aperture - absorber

Another important factor is dimensioning of the aperture. A compromise has to be found between an aperture big enough to let all the solar beams from the heliostat field enter and one as small as possible to reduce thermal losses through the aperture. Since aperture dimensions influence the view factors needed for calculation of IR radiation and solar reflection losses, a simplified approach for the view factors in dependence on the aperture dimensions was derived.

Optimization of the aperture was done by combining sbpRAY with another sbp tool called sbpOpt. This optimizer searches for the minimum of a value by changing input parameters between certain upper and lower bounds. The optimization algorithm can be adjusted easily. For the project shown here, the Method of Moving Asymptotes (MMA) was used [8]. The aperture dimensions were used as inputs and the negative net absorber output power as the output.

The optimization showed a noticeable impact on the net output power. Depending on initial dimensions, the optimization could improve net output power up to several percent. Figure 11 shows an exemplary aperture optimization. The viewing angle is oriented parallel to the aperture frame. The rectangular red frame represents the initial manually adjusted aperture. The green frame shows the first result of automatic optimization, maintaining the rectangular form for the sake of faster calculation. In a further optimization step, the aperture form was adapted to better meet the requirements (yellow).

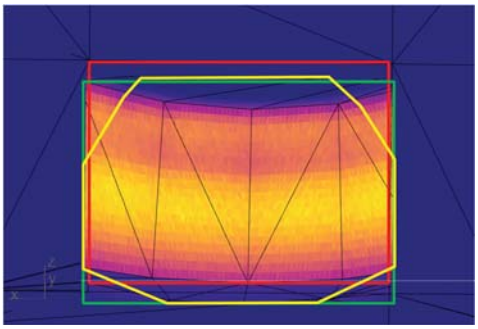

FIGURE 11. Exemplary aperture optimization (red: initial aperture, green: optimized aperture – step 1, yellow: optimized aperture – step 2)

Figure 12 shows the solar field with colour coded heliostat efficiencies. Gebreiter et al. discusses the calculation of heliostat efficiencies and receiver flux with sbpRAY in more detail [1]. It can be seen that the efficiency decreases with the distance from the cavity receiver. Also, slip planes can be detected, not only due to the slightly increased distance to the row in front of the slip plane, but also due to the lower efficiency which some heliostats show in these rows. Furthermore, it can be seen that heliostats at the outer sides have lower efficiencies.

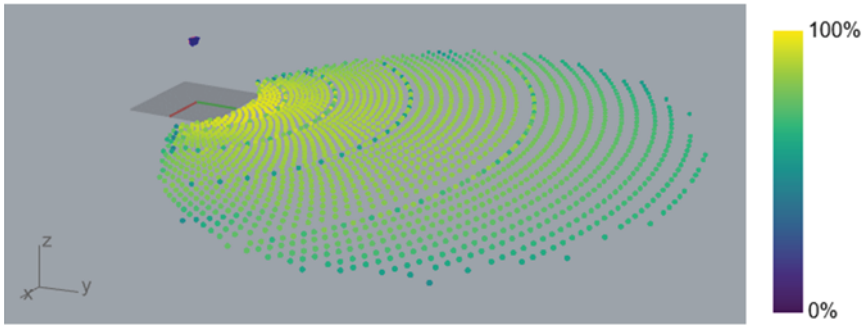

FIGURE 12. Receiver and solar field for Next-CSP, view from Rhino

PARAMETER STUDIES

A factor with considerable influence on the net output power is the height of the tower (receiver). With the simulation tools described, a comparison between different tower heights could be performed easily. Firstly, the heliostat field was optimized for each tower height; for better comparison with the same number of heliostats. At the beginning, the same receiver was used for each simulation (optimized for a tower height of 93 m). Figure 13 gives an overview on the impact of tower height on net output power, receiver and field efficiency. There is a considerable effect on heliostat field efficiency and, as the receiver stays unchanged, a small effect on receiver efficiency.

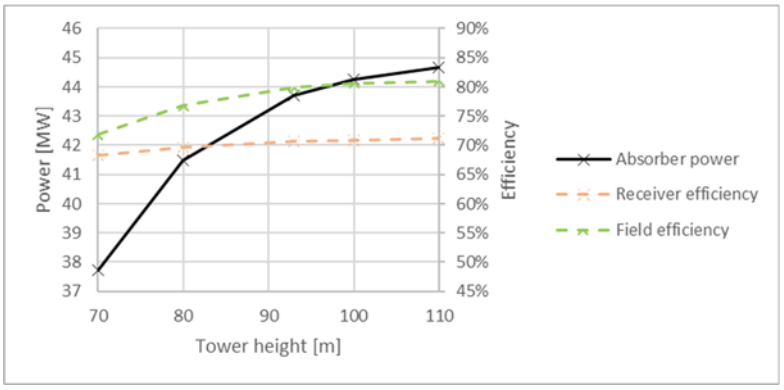

FIGURE 13. Impact of tower height with adjusted heliostat field

In the next step, optimized receivers were simulated; results are shown in Fig. 14. It can be seen that optimization of the receiver, especially optimization of the receiver aperture, is necessary to obtain higher efficiencies and get a fair comparison between the different tower heights. The slightly smaller receiver efficiencies below 90 m comparing Fig. 14 to Fig. 13 is the result of a compromise between an aperture size optimal for the solar field (as big as possible to maximize the input from the field while getting a homogenous flux on the absorber) and one optimal for the receiver efficiency (as small as possible to minimize receiver losses). Regarding the course of the solar field efficiency over tower height, a slight decrease can be seen at tower heights lower than 80 m. The decreasing gradient of power output and field efficiency for larger towers are an indication that with fewer heliostats the power output would decrease less than for lower towers. The reason for this is that for large tower heights aim points must be shifted from the centre to the sides of the absorber to avoid excessive flux in the centre. This leads to degraded performance of the affected heliostats. A linear approximation, pictured in Fig. 14, leads to an average increase of 0.155 MW/m in the examined range.

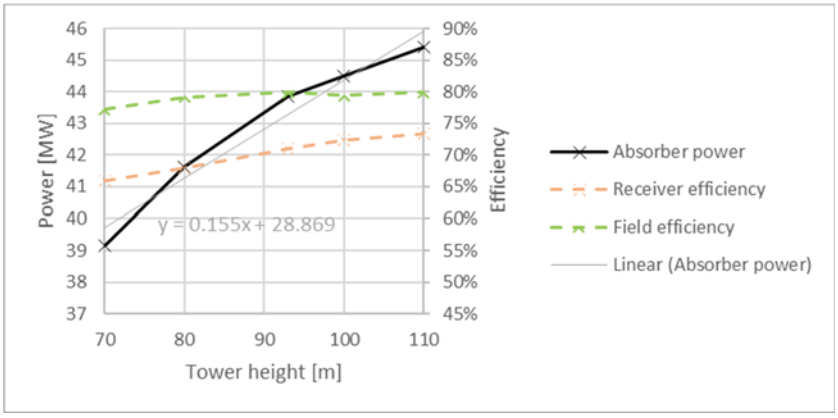

FIGURE 14. Impact of tower height with optimized receiver

For final decision on the tower height not only the absorber output has to be regarded but also height dependent heat losses due to particle transport and costs. A rough techno-economic cost analysis (not including heat losses in the transport system but focused on the tower itself) resulted in specific costs of 180 €/kW_{th} (cost for the additional tower height between 70 and 110 m regarding particle elevator, construction site equipment, foundation, tower structure with platforms and a passenger lift) which indicates that higher towers are profitable.

Additional parameters beyond geometry have significant impact on the net power output and should be considered in the planning process: Cavity and absorber material parameters as well as heliostat quality (Fig. 15). The absorber tube absorptivity for solar radiation has the biggest influence while the impact of the other analysed parameters is rather small. The corresponding values are listed below.

Solar reflectivity of ceramic cavity walls: 0.03 % receiver efficiency / % reflectivity
Emissivity of ceramic cavity walls: 0.0007 % receiver efficiency / % emissivity
Solar absorptivity of absorber: 0.58 % receiver efficiency / % absorptivity
Emissivity of absorber: -0.03 % receiver efficiency / % emissivity

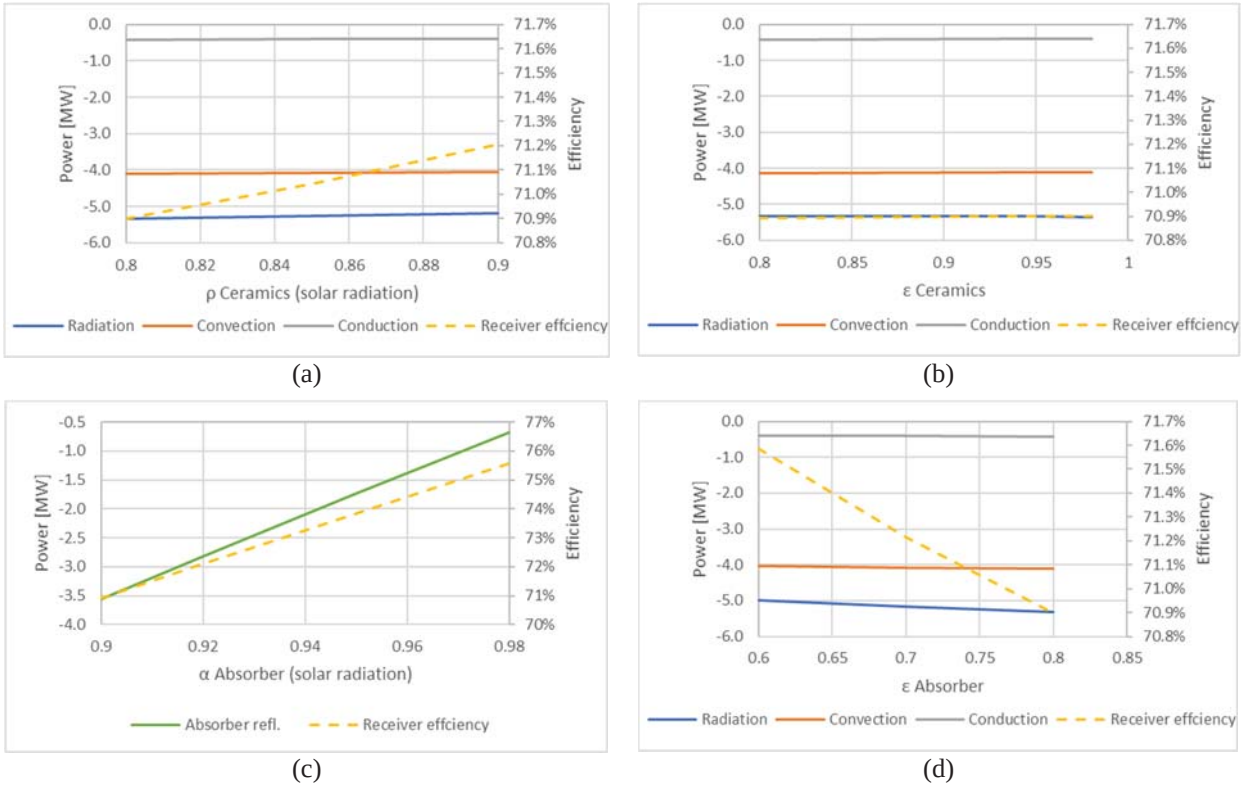

FIGURE 15. Impact of material parameters (a) Solar reflectivity of ceramic walls (b) Emissivity of ceramic walls (c) Solar absorptivity of absorber (d) Emissivity of absorber

When selecting the absorber paint, attention should be paid not only to absorptivity in new condition but also to the effect of UV radiation and weathering (usual absorber coatings show considerable degradation within few years).

Figure 16 depicts the influence of heliostat parameters on power output, field and receiver efficiency. Using a linear approach, the respective values are as follows:

Slope error (2D): -0.7 % output power / 0.1 mrad slope error 2D
Reflectivity: 1.2 % output power / % reflectivity
Tracking error: -1.1 % output power / 0.1 mrad tracking error 1D
Cleanliness: 1.3 % output power / % cleanliness

The influence is considerable. Especially the two parameters reflectivity and cleanliness have significant impact. Nevertheless, cleanliness is merely included for informative reasons, as it is not related to the design of the heliostat.

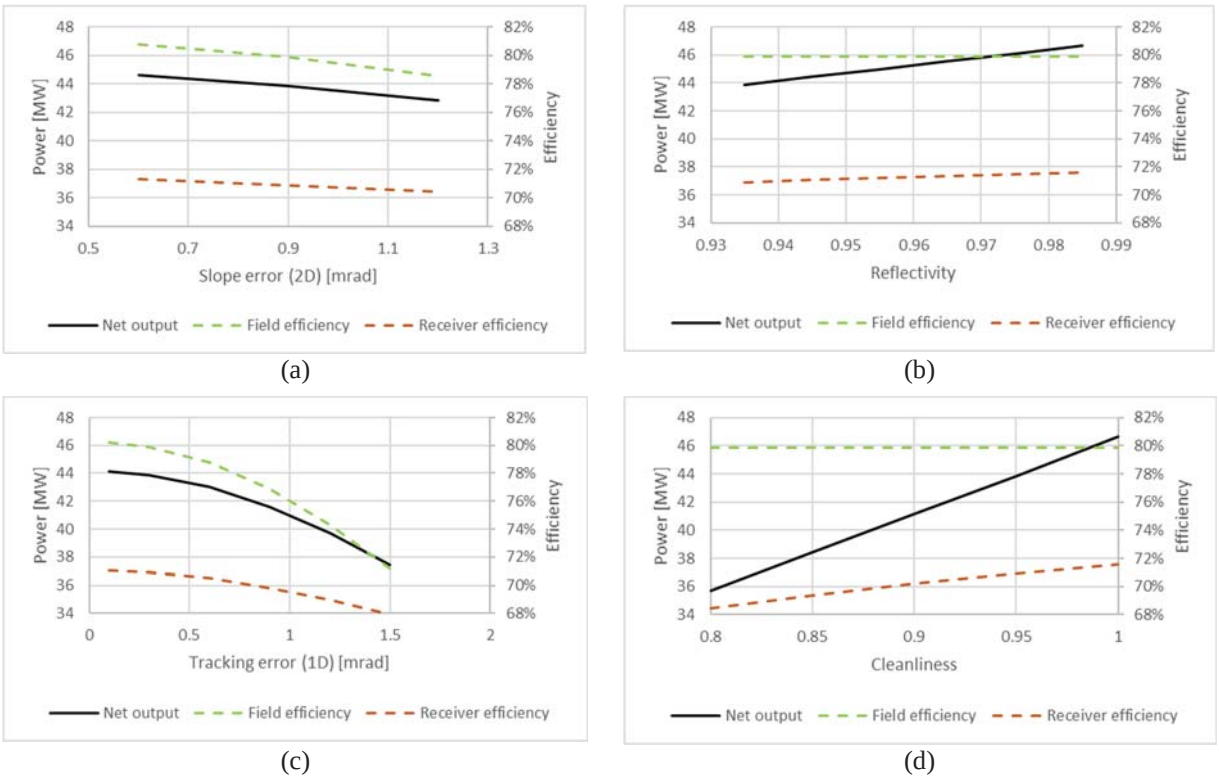

FIGURE 16. Impact of heliostat parameters (a) Slope error (2D) (b) Reflectivity (c) Tracking error (1D) (d) Cleanliness

CONCLUSION

The study concluded that to reach a high receiver efficiency, the receiver needs to be adapted according to the application. To find the optimal configuration which enables the highest product of optical and thermal receiver efficiency, more effort is required. High quality heliostats and a sufficiently high tower as well as suitable cavity materials and receiver coating with good properties are key prerequisites. With the presented extension of sbpRAY for the simulation of cavity receivers, a simple, flexible and powerful simulation program is available for this application. The program is well suited for parameter studies and can set the basis for techno-economic optimizations.

REFERENCES

1. Next-CSP – High temperature concentrated solar thermal power plant with particle receiver and direct thermal storage [Online] 2016. [Cited: 13.05.2019] *http://next-csp.eu/*
2. D. Gebreiter, G. Weinrebe, M. Wöhrbach, F. Arbes, F. Gross, W. Landman, "sbpRAY – A Fast and Versatile Tool for the Simulation of Large Scale CSP Plants," in *Solar PACES Annual Conference 2018*, Casablanca.
3. R. McNeel and Associates, "Rhinoceros," [Online] 2019. [Cited: 29.04.2019] *https://www.rhino3d.com*
4. F. von Reeken, G. Weinrebe, T. Keck, M. Balz, "Heliostat cost optimization study," in *AIP Conference Proceedings 1734*, 160018, Solar Paces Conference 2016, Cape Town.
5. J. Greenwood, "The correct and incorrect generation of a cosine distribution of scattered particles for Monte-Carlo modelling of vacuum systems," in *Vacuum 67* (2002).
6. A.M. Clausing, "Convective Losses From Cavity Solar Receivers – Comparisons Between Analytical Predictions and Experimental Results," in *Journal of Solar Energy Engineering 105*, pp. 29-33 (1983).
7. J. Samanes, J. García-Barberena, F. Zaversky, "Modeling Solar Cavity Receivers: A Review and Comparison of Natural Convection Heat Loss Correlations," in *Energy Procedia 69*, pp. 543-552 (2015).
8. R.E. Perez, P.W. Jansen, and J.R.R.A. Martins, "pyOpt: A Python-Based Object-Oriented Framework for Nonlinear Constrained Optimization," in *Structures and Multidisciplinary Optimization 45(1)*, pp. 101-118 (2012).